Eur. Phys. J. B **17**, 371–383 (2000)

THE EUROPEAN PHYSICAL JOURNAL B

EDP Sciences

Chord length distributions and small-angle scattering

W. Gille[a]

Department of Physics, Martin-Luther-University Halle-Wittenberg, SAS-Laboratory, Hoher Weg 8, 06120 Halle, Germany

Received 15 March 1999 and Received in final form 26 April 2000

Abstract. Chord length distributions describe size, shape and spatial arrangement of geometrical objects (particles). The chord length distribution is in principle proportional to the second derivative of the correlation function of small-angle scattering. It is calculable from a relative measurement of the scattering intensity $I(h)$. In structure research, the characterization of numerous particle systems can be achieved by comparing experimental chord distributions with theoretical ones, provided the latter are available with sufficiently high precision for a lot of fundamental, universal shapes. Both sides of this concept are exemplified: - the step from a relative measurement of the scattering intensity of an isotropic two-phase sample to the chord length distribution (errors in $h_{\rm k}$ and in $I_{\rm k}$, limited h-interval, corresponding to the region $(1-2)$ nm $< r$ in real space, must be observed); as well as the geometric matter of calculation of chord distributions as fingerprints for basic geometric figures, including the non-convex case.

PACS. 61.10.Eq X-ray scattering (including small-angle scattering) – 61.12.Ex Neutron scattering techniques (including small-angle scattering)

1 Introduction

Chord distributions are fundamental functions in many various fields: microdosimetry, dosimetry of internal emitters, detector response and radiation shielding, stereological analysis of two-dimensional sections in electron microscopy, quantitative image digitalization and the acoustical design of auditoria, geometric and dielectric characterization of porous media, investigations of electric conductivity and transport, and relaxation phenomena in porous media [1–6].

There exist physical apparatuses in structure research which indirectly measure the distribution law of random chords of a three-dimensional sample. This corresponds to the practical stereological situation where an isotropic sample containing particles of unknown size and shape and arrangement is interradiated by a beam of monochromatic X-ray light.

In material research, microheterogeneities (sizes from some nanometres up to some hundred nanometres) of selected materials are investigated by scattering methods. One of the structure functions resulting from such experiments is the chord length distribution (c.l.d.). c.l.d.'s are obtained, whenever a geometric figure of any dimension is randomly intersected by straight lines. The investigation of c.l.d.'s is a special geometric matter; for the general case see Stoyan *et al.* [1], Serra [2] and Cabo and Baddeley [7]. Chord length distributions can be defined for any geometric object. They reflect the size and the shape of the object.

[a] e-mail: gille@physik.uni-halle.de

There are different methods for the formulation of the c.l.d.'s from the viewpoint of geometric probabilities [1,2,8]. In order to avoid problems here, the mere definition of the distribution function of a random chord length variable ξ, $\mathrm{F}(\ell) = Pr(\xi < \ell)$ should always be used.

The information in a Small-Angle Scattering curve, SAS-curve $I(h)$ of nanometer particles, can be used for shape and size characterization *via* correlation function, c.f. $\gamma(r)$, of SAS, Guinier and Fournet [9], Feigin and Svergun [10] and Tchoubar [11]. The connection between an SAS-experiment of a realistic two-phase sample and the c.l.d. of stochastic geometry is based on the following. The atomistic construction of the matter determines an upper scaling limit in SAS. Below that, particle borders have no geometrical sense. The distances between single scattering centres are not resolved in the SAS experiment. Therefore, the sample-densities in the r-interval $r_{\rm min} < r$ can be approximated by piecewise continuous functions. The practicable limit is $r_{\rm min} = (1-2)$ nm. Thus, for the geometrical description of particle models in space the fine structure of the particle surfaces, $r < r_{\rm min}$, is completely smoothed out.

The outline of this review article is the following. Section 1.1 compares the so-called distance distribution density function $p(r)$ of a particle (see [10] on pages 40-42), with the c.l.d. While $p(r)$ reflects all distances between the scattering centres of an isotropic two-phase particle arrangement in the sample, the set of intercepts exclusively reflects distances between *interfaces of particles*. Here, the strategy which connects the c.l.d. $A(\ell)$ in terms

of γ'' can be introduced in the simplified form

$$A(\ell) \equiv f_\mu(\ell) = \overline{\ell}\gamma''(\ell)$$
$$f_\nu(\ell) = \ell\gamma''(\ell). \quad (1)$$

Only a single conversion element is necessary in equation (1), and the second derivative of the small-angle scattering correlation function (c.f.) allows the determination of the set of c.l.d.'s f_μ, f_ν. Section 1.2 explains the connection between the scattering experiment and $\gamma''(r)$. The functions f_μ and f_ν describe two different types of randomness for the intersection of straight lines with geometric forms, see Section 2. Section 3 explains some $A(\ell)$-examples of elementary figures.

If the mean distances between two adjacent particles are relatively small (relatively high volume fraction), two types of μ-chords exist. An extension of equation (1) for isotropic particle arrangements will be considered in Section 4.

It is useful to describe a two-phase particle system with the so-called indicator function $i(\mathbf{r})$, which is 1 within and 0 outside the particle phase [1], instead of local densities in each point in real space. For arrangements of all kinds of such smooth model-particles the basic law $I(h) \approx h^{-4}$, if $h \to \infty$, holds. This is highly valuable information for data evaluation, for the step from $I(h)$ to γ'', see [10,12] and for more details Sobry and Ciccariello [13–15]. In Section 5 three examples concerning the step from $I(h)$ to γ'' will be explained.

Considerations of c.l.d.'s for non-convex figures are relatively rare. Section 6 will deal with this case and consider particles with hollow parts. Finally, Section 7 investigates a long-standing problem: the analysis of the behaviour of $A(\ell)$ near the largest particle dimension $\ell = L$. Strategies for a direct estimation of L from the c.f. are included.

1.1 The distance distribution density p(r) and the c.l.d. A(ℓ)

Among many possibilities there exist the following two to "*indicate*" particles.

1. The particles may be considered and analyzed as the sum of all their volume elements $\mathrm{d}V_\mathrm{i}$. Analysing the distances r_i between all points of the particle volume(s), the distance distribution density $p(r)$ of the particle, see [9,10], results. The connection between $\gamma(r)$ and $p(r)$ is given for any particle shape, involving a whole volume V_0, by $p(r) = 4\pi r^2\gamma(r)/V_0$. For convex particles the moments of $A(\ell)$ can be expressed and interpreted by those of $p(r)$, see Damaschun and Pürschel [16].

2. Each smooth particle can be defined by use of a well-defined border with finite surface area, see Figure 1. In this case, the border distribution function $p_\mathrm{b}(r)$ of the particle border can be given, but it is more convenient to operate with c.l.d.'s, reflecting the features of the interface(s) between one or more particles. Evidently, c.l.d.'s are not influenced at all by the inner parts of the particle(s); they are much more shape-sensitive than $p(r)$. In fact, merely the analysis of the interfaces of any single particle leads to an asymptotic expansion for its scattering behaviour, which is sometimes an excellent approximation in an unexpectedly wide h-region of the scattering curve of the particle, Sobry [14]. There exist fully developed theories, see Lu and Torquato [17] and [11,18,19], for the interpretation of the c.l.d. in tightly packed isotropic two-phase systems, which in principle all go back to the so-called linear integration principle of Rosiwal [20]. The volume fraction of a two-phase particle system is clearly defined by the mean chord lengths of the particle-phase and the intermediate-phase (often called matrix phase), see Section 4.

1.2 Scattering experiment, c.f. and c.l.d.

All structure parameters, defined in the field of SAS, including the volume fraction, can be directly put down to the c.l.d.'s [20]. The normalized c.f., $\gamma(0) = 1$, follows from $I(h)$ by use of a transformation

$$\gamma(r) = \frac{\int_0^\infty h^2 I(h) \frac{\sin(hr)}{hr} \mathrm{d}h}{\int_0^\infty h^2 I(h) \mathrm{d}h}\,. \quad (2)$$

An example of a direct determination of the c.l.d. from $I(h)$, based on equations (2,1), is to operate with

$$\gamma''(\ell) = \frac{\frac{1}{l^2}\int_0^\infty [h^4 I(h)]'' \frac{\sin(h\ell)}{h\ell} \mathrm{d}h}{\int_0^\infty h^2 I(h) \mathrm{d}h}, (1.5-2)\mathrm{nm} \le \ell \le \ell_{\max}, \quad (3)$$

which is one selected synonymous representation. Equation (3) is based on the differentiation of equation (2), followed by integration by parts [12]. Equation (3) holds true if the particle system consists of two phases (two different densities) with smooth inner boundary surfaces. From equation (3) the set of c.l.d.'s. can be obtained from appropriate experiments, see Section 5.

The fundamental equation (1) can be used in the transparent single-particle case, see next section, as well as, in principle, for particles with hollow parts or for tightly packed particle arrangements. Of course, a lot of special problems, concerning the details of this concept, are of interest to this technique of data evaluation in SAS, for the comparison of model-c.l.d.'s with experimental ones, see Gille [18,19]. Here it is remarkable that Guinier and Fournet [9], have proposed one special chord-type and Tchoubar [11], has explained two chord-types. Now, the three basic types of c.l.d.'s will be explained in the next section.

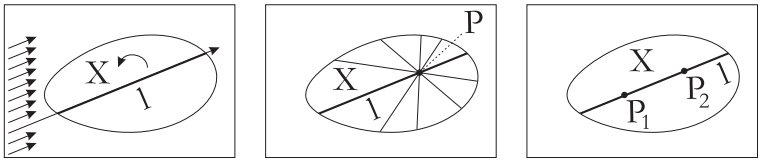

Fig. 1. a) μ-chords, $f_\mu(\ell) \equiv A(\ell)$: Isotropic-Uniform-Random-chords, IUR-chords arise if X is evenly rotated in all directions in space within a field of straight lines. This situation directly corresponds to the determination of $I(h)$ for the SAS experiment of a so-called *isotropic* system. Here, each differentiation step of $\gamma(\ell)$ corresponds to one end of the IUR-chord l, see Enns and Ehlers [21] and Teichgräber [22] and Fanter [23]. b) ν-chords, $f_\nu(\ell)$: Weighted randomness chords arise if, after a choice of evenly distributed points within X, straight lines are defined for each point having IUR-orientation. In many fields of radiation research and dosimetric considerations the term I-chord-randomness or Interior Radiator Randomness (IRR) is used. c) λ-chords, $f_\lambda(\ell)$; Two-point-random-chords result if a chord is defined by two independent points P_1, P_2 which are evenly distributed in X.

2 Geometric definitions of the c.l.d. of a single particle

There exist different types of randomness for the intersection of a convex body by straight lines. Mainly three types of chords are in use, which appear in well-investigated circumstances. Figure 1 explains μ-, ν-, and λ-chords in the case of any convex geometric figure X.

These c.l.d.-types are connected, in the case of any convex X, with volume V and surface area S by, see [11,13,15,18,22,23]:

$$A(\ell) \equiv f_\mu(\ell) = \frac{4V}{S}\frac{1}{\ell} f_\nu(\ell) = \frac{12V^2}{\pi S}\frac{1}{\ell^4} f_\lambda(\ell). \qquad (4)$$

Equation (4) also holds true in the case of non-limited sets X, for example for infinitely long cylinders or for a layer. The first moment of $A(\ell)$ used in equation (4) corresponds to a special case of Cauchy's formulæ: denoting the spatial orientation angles of a chord direction by the random angle-variables α (horizontal angle, equally distributed in $(0,2\pi)$) and by θ (angle to a fixed z-axis in the particle, distributed with density $\cos(\theta)/(\pi/2)$), then the ratio of V and the projection area of the particle $S_p(\alpha,\theta)$, averaged over all IUR-directions, gives Cauchy's conversion factor $4V/S$. It was also used in equation (1). The representation equation (5) is more compact, but see equations (21, 24).

$$\overline{\ell} = \frac{V}{\overline{S_p(\alpha,\theta)}}\,. \qquad (5)$$

Initially, ν-chords $f_\nu(r) = g(r)$ were introduced into structure research in [9] under the formal name "chord distribution". Later works introduced a clear connection between SAS and μ-chords. This is the basis for the computer-chord-simulation, see [22,23].

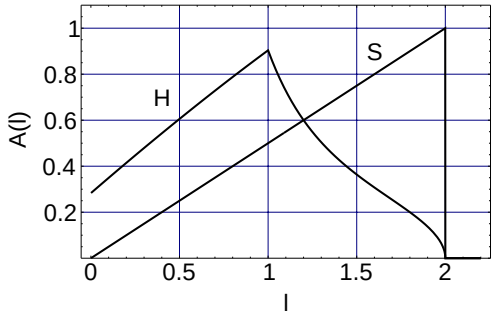

Fig. 2. Sphere (S) and hemisphere (H) with the same radius $R = 1$. Here it is directly possible to recognise the biggest diameter of the particle, $L = 2$. But in other cases this is not possible, see Figures 14 and 21.

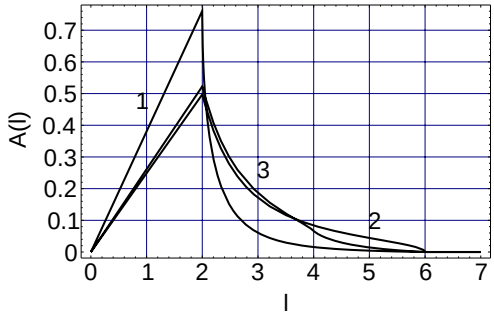

Fig. 3. Ellipsoids, $L = 6$, with semi-axes {a,b,c}: (1){1,1,3}, (2){1,3,3}, (3){1,2,3}. The small differences between (2) and (3) would be undetectable in such plots if exclusively the c.f. or the distance distribution of these particles were analyzed.

3 A(ℓ)-functions of elementary geometric figures

3.1 Fingerprint properties of selected geometric shapes

The Figures 2–5 show μ-c.l.d.'s of selected geometric shapes. Each behaviour of $A(\ell)$ has its specific peculiarities and is a geometric fingerprint of the interface of the particle [22–31].

The situation that two different three-dimensional figures possess the same c.l.d. has been unknown until

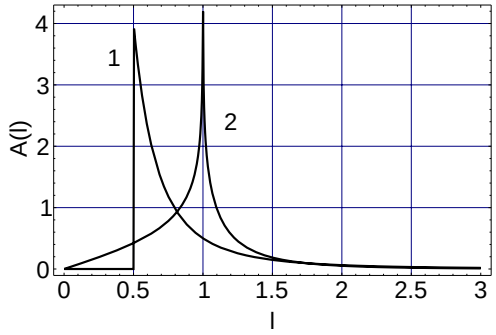

Fig. 4. Infinitely long cylinder $D = 1$, curve (1), and lamella $H = 1/2$, curve (2) with the same mean chord length $\overline{\ell} = 1$. The general cylinder-case was studied by Gille [8].

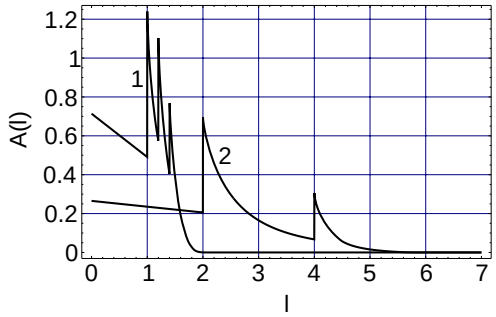

Fig. 5. Parallelepipeds with edges {a,b,c}: (1){1,1.2,1.4}, $L = 2.097$ and (2){2,3,∞}, limiting case of a rectangular bar. In both cases the exact L is undetectable from $A(\ell)$, see Ciccariello [15]. Here, $A'''(\ell)$ must be considered in order to study L. The spectrum of possible a,b,c - combinations is far-reaching, see [27,31].

today. The case of arrangements of particles with a size distribution and their c.l.d. was considered in detail by Fanter [23].

A new quality results, in the case of non-convex figures or figures with hollow parts, or if chords between the particles have an influence in the particular r-interval under consideration. This will be studied in the Sections 3.2–3.5. and in Section 4.

3.2 The hemisphere case: an example of an analytic representation of A(ℓ)

For analytical representations of c.l.d.'s, interval splittings are indispensable, see [27] and Gille and Handschug [28]. The $A(\ell)$-function of a hemisphere with radius R can be written in a compact form without any approximation, but see also Enns and Ehlers [21].

A detailed explicit solution, including an analytical representation of the c.f., was calculated lastly, see [28,29]. $f_\mu(\ell)$, see Figure 2, consists of two independent parts. On the one hand, basic-chords which hit the base surface of the hemisphere are considered. Independent of these, on the other hand, those chords which do not hit the basic surface, the cap-chords, are investigated likewise. Considering the mean projection planes of the hemisphere into a direction perpendicular to the chord direction follows.

The probability that a μ-chord is a cap-chord is 1/3. The probability that a μ-chord is a basic-chord is 2/3. Both chord types possess their own distribution densities, see [28]. The final result for all chords, obtained from both parts by averaging, writes as follows:

1. Interval $0 < \ell \leq R$

$$f_\mu(\ell) = \frac{2}{3}\frac{\ell}{R^2} + \frac{1}{\pi R}\sqrt{1-\frac{\ell^2}{4R^2}} + \frac{2R}{3\pi\ell^2}\left[\sqrt{1-\frac{\ell^2}{4R^2}} - \frac{2R}{\ell}\arcsin\left(\frac{\ell}{2R}\right)\right]. \quad (6)$$

2. Interval $R \leq \ell \leq 2R$

$$f_\mu(\ell) = \frac{1}{\pi R}\sqrt{1-\frac{\ell^2}{4R^2}} + \frac{2R}{3\pi\ell^2}\left[\sqrt{1-\frac{\ell^2}{4R^2}} + \frac{2R}{\ell}\arccos\left(\frac{\ell}{2R}\right)\right]. \quad (7)$$

The author doesn't know another simple geometric figure possessing exactly this c.l.d. In this light, some distinctive derivatives of $A(\ell)$ at special ℓ-positions are summarized now. Contrary to the sphere, to the cone and to the cuboid, this result, equations (6, 7), see Figure 2, is continuous in $0 < \ell < 2R$, and particularly, too, at transition positions $\ell = R$ and $\ell = 2R$. It holds that:

$$f_\mu(0+) = \frac{8}{9\pi R}. \quad (8)$$

The largest particle dimension $L = 2R$ can be detected from the left-hand derivative of $f_\mu(2R)$, which equals $-\infty$ here. This detail differs extremely from the behaviour obtained for other geometric figures, see also Stoyan and Stoyan [8], pp. 135-138. The global maximum of $f_\mu(\ell)$ lies at $\ell = R$. Also the position $\ell = \sqrt{2}R$, possessing the f_μ-values

$$f_\mu(R) = \frac{15\sqrt{3}+8\pi}{18\pi R}, \quad f_\mu(\sqrt{2}R) = \frac{8+\pi}{6\sqrt{2}\pi R}, \quad (9)$$

is specific for this shape. The left-hand and the right-hand derivatives $f'_\mu(R\pm)$ are

$$f'_\mu(R\pm) = \frac{-25\sqrt{3}\mp 24\pi}{18\pi R^2}. \quad (10)$$

The first two derivatives of $f_\mu(\ell)$ at $\ell = \sqrt{2}R$ are the following:

$$f'_\mu(\sqrt{2}R) = -\frac{16+3\pi}{12\pi R^2}, \quad f''_\mu(\sqrt{2}R) = \frac{\sqrt{2}(2+\pi)}{2\pi R^3}. \quad (11)$$

From equations (6, 7, 10, 11) follows the existence of a point of inflexion of $f_\mu(\ell_\mathrm{i})$ in $\sqrt{2}R < \ell_\mathrm{i} < 2R$. From equations (6, 7) it follows that the theoretical relations for the moments of f_μ are in agreement with the theory $M_0 = 1$, $M_1 = 4V/S$ and $M_4 = 12V^2/(\pi S)$. The second moment M_2 equals R^2. A general form for M_2 is still unknown.

3.3 One-Chord Distribution and Multi-Chord Distributions (OCD and MCD)

In the case of particles containing one or more hollow parts, it is a good idea to consider two different types of distributions. The MCD-type, the natural case of SAS, see Porod [32], is generated if each chord-length-segment is taken for itself. On the other hand, it can be useful to consider *the sum of all chord segments* through the particle on one straight line as the random variable. This is the OCD-case, $\ell = \ell_1 + \ell_2 + \ell_3 + \ldots$ The following examples use the abbreviation:

$$x = |term(\ell)|_a^b \quad \text{stands for:} \quad x = term(\ell), \\ \text{if } a < \ell < b, \text{ else } x = 0. \tag{12}$$

3.4 Hollow sphere of diameter d with central hole of inner diameter d_i and the corresponding plane figure, the circular ring

The c.l.d. of the hollow sphere in the MCD-case is, see Figure 7:

$$A_\mathrm{MCD}(\ell) = \left| \frac{2\ell}{d^2 + d_\mathrm{i}^2} \right|_0^{\sqrt{d^2 - d_\mathrm{i}^2}} \\ + \left| \frac{4\left[\left(\frac{d^2}{4} - \frac{d_\mathrm{i}^2}{4} \right)^2 - \ell^4 \right]}{\ell^3 (d^2 + d_\mathrm{i}^2)} \right|_{\frac{d-d_\mathrm{i}}{2}}^{\frac{\sqrt{d^2 - d_\mathrm{i}^2}}{2}} . \tag{13}$$

The c.l.d. of the hollow sphere in the OCD-case is, see Figure 6:

$$A_\mathrm{OCD}(l) = \left| \frac{2l}{d^2 + d_\mathrm{i}^2} \right|_0^{\sqrt{d^2 - d_\mathrm{i}^2}} + \left| \frac{\left(d^2 - d_\mathrm{i}^2\right)^2 - \ell^4}{\ell^3 \left(d^2 + d_\mathrm{i}^2\right)} \right|_{d-d_\mathrm{i}}^{\sqrt{d^2 - d_\mathrm{i}^2}} . \tag{14}$$

The sphere, diameter $d = 4$, with central void, diameter $d_\mathrm{i} = 2$, is considered in Figures 6, 7. The first moments of the c.l.d.'s are 1.87 in the MCD-case and 2.35 in the OCD-case. These special results coincide with the modified Cauchy theorem

$$\overline{\ell}_\mathrm{MCD} = \frac{4V}{S}, \quad \overline{\ell}_\mathrm{OCD} = \frac{4(V_\mathrm{c} + V_2)}{S} . \tag{15}$$

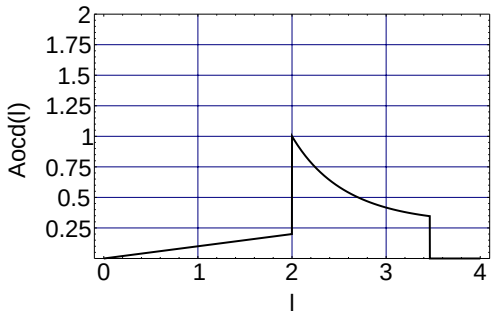

Fig. 6. OCD of a hollow sphere.

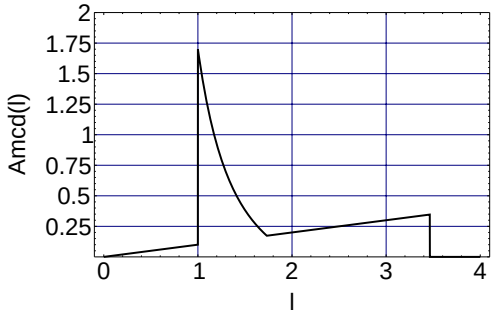

Fig. 7. MCD of a hollow sphere.

S is the whole (inner plus outer) surface. In this light, the modification in equation (15), exclusively necessary in the OCD-case, consists in a splitting of the numerator-volume-term into a sum of two different volumes. The part V_c is the volume of the convex region (sphere volume minus the common volume of the sphere with a long circular cylinder of diameter d_i) and part V_2 is *double* the volume of the non-convex region of the hollow sphere (common volume of a long cylinder of diameter d_i minus the volume of the central void).

3.5 Circular ring of diameter d with central circle of inner diameter d_i

Here, poles in the c.l.d.'s occur. This behaviour is well-known referring to the c.l.d.'s of the sphere and of a circular area. The c.l.d. in the MCD-case is, see Figure 9:

$$A_\mathrm{MCD}(\ell) = \left| \frac{\ell}{(d + d_\mathrm{i})\sqrt{d^2 - \ell^2}} \right|_0^{\sqrt{d^2 - d_\mathrm{i}^2}} \\ + \left| \frac{2d_\mathrm{i}}{d + d_\mathrm{i}} \frac{(d^2 - d_\mathrm{i}^2)^2 - 16\ell^4}{16 d_\mathrm{i}^2 \ell^3 \sqrt{1 - \frac{\left(\frac{d^2}{4} - \frac{d_\mathrm{i}^2}{4} - \ell^2\right)^2}{d_\mathrm{i}^2 \ell^2}}} \right|_{\frac{d-d_\mathrm{i}}{2}}^{\frac{\sqrt{d^2 - d_\mathrm{i}^2}}{2}} . \tag{16}$$

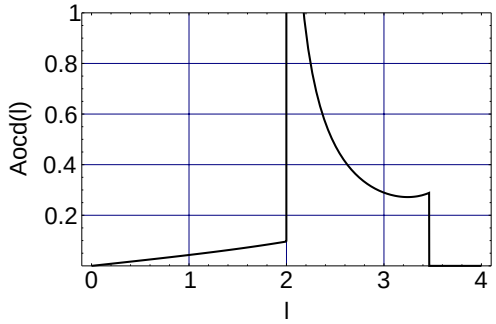

Fig. 8. OCD of a circular ring.

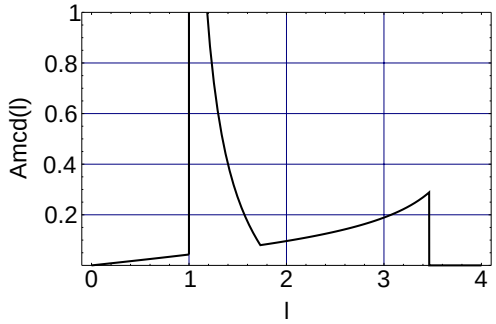

Fig. 9. MCD of a circular ring.

The c.l.d. in the OCD-case is, see Figure 8:

$$A_{\mathrm{OCD}}(\ell) = \left| \frac{\ell}{(d+d_\mathrm{i})\sqrt{d^2-\ell^2}} \right|_0^{\sqrt{d^2-d_\mathrm{i}^2}} + \left| \frac{2d_\mathrm{i}}{d+d_\mathrm{i}} \frac{(d^2-d_\mathrm{i}^2)^2-\ell^4}{4d_\mathrm{i}^2\ell^3\sqrt{1-\frac{\left(d^2-d_\mathrm{i}^2-\ell^2\right)^2}{4d_\mathrm{i}^2\ell^2}}} \right|_{d-d_\mathrm{i}}^{\sqrt{d^2-d_\mathrm{i}^2}} . \quad (17)$$

The extension of the Cauchy theorem for a plane figure, equation (18), is analogous to equation (15)

$$\overline{\ell}_{\mathrm{MCD}} = \frac{\pi S}{u}, \quad \overline{\ell}_{\mathrm{OCD}} = \frac{\pi(S_\mathrm{c}+S_2)}{u} \quad (18)$$

with whole perimeter u and with the surfaces S_c, S_2. The Figures 8, 9 show plots in the case $d = 4$, $d_\mathrm{i} = 2$. The first moments of these c.l.d.'s are $1/\sqrt{3}+5\pi/9$ in the OCD-case and $\pi/2$ inthe MCD-case.

The basic form of equation (15) and equation (18) is unchanged for similar non-convex figures, see [19]. This also includes the case that the void has a more compact form or is not placed in a central position. Certainly, averaged numerator-terms in equations (15, 18) will be used then.

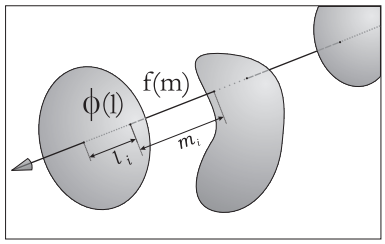

Fig. 10. One straight test line intersects particles in a two-phase system with about $p = 20\%$. Chord lengths ℓ_i (within the particles) and m_i (outside the particles) result. On the other hand a sequence of sum-possibilities, like $\ell_\mathrm{i}+m_\mathrm{i}$, $m_\mathrm{i}+\ell_\mathrm{i}$ or $\ell_\mathrm{i}+m_\mathrm{i}+\ell_\mathrm{i}$ or $m_\mathrm{i}+\ell_\mathrm{i}+m_\mathrm{i}$, indicate details of the particle arrangement, and details of the packing-characteristic of the particles, see [18]. Both effects are mixed in one function γ''.

4 Particle arrangements with a volume fraction p

In the case of a tightly packed arrangement of particles, two types of chord segments (denoted by ℓ_i and m_i, see Fig. 10) exist, alternating on a sufficiently long test line through the system. In cases $p \to 0$ it is more difficult, sometimes unrealistic, to observe extremely long m_i-segments. But, m_i-segments always exist in practice.

4.1 The distribution densities $\phi(\ell)$ and f(m) for the isotropic case

The chord segments on one testline alone reflect a great variety of information about the particle arrangement and p. According to the standpoint of Tchoubar [11], here two basic c.l.d.'s exist, named $\phi(\ell)$ and $f(m)$. Both distribution densities are closely connected with the function $\gamma''(r)$. The identity $\phi(\ell) \equiv \mathrm{A}(\ell) \equiv f_\mu(\ell)$ holds in the special case $p = 0$; $f(m) \to 0$is not considered then.

If particles of a typical extent of 10 nm (at about 50% volume fraction) are supposed in a sample of the thickness $(0.1-1)$ mm, then already one straight line in the direction of the primary beam intersects $10^4 - 10^5$ particles. Thus, there exist more than 10^8 chord segments in the irradiated volume of a realistic neutron or X-ray primary beam; this is more than enough for a statistical description strategy of the irradiated sample volume. Consequently, the theorems of differential calculus are applicable. Here, Dirac's δ-function must appear as a result of the differentiation of the $\gamma(r)$ singularities at the particle borders. The simplest example for the appearance of a δ-function is the rod of length L with the c.f. $\gamma_R(r, L) = 1 - r/L$, if $r < L$ and $\gamma_R(r, L) = 0$, if $r > L$. Here, the function γ_R'' is given by: $\gamma_R''(r, L) = \delta(r - L)$. *It does not include any information* about the distances $r < L$ at all. In all cases known, γ'' is simpler to represent than γ, as a consequence of geometry.

4.2 Connections between $\phi(\ell)$, f(m) and γ''(r)

If l_i and m_i are random variables which are independent of each other, a general connection

$$\overline{\ell}(1-p)\gamma''(r) = [\phi(r) + f(r) - 2\phi(r)*f(r))]* \\ [\delta(r) + (\phi(r)*f(r)) + (\phi(r)*f(r))^{2*} + \ ... + ..] - 2\delta(r) \tag{19}$$

holds true. Equation (19) is an approximation for the mutually dependent ℓ_i, m_i. The symbol "$*$" stands for the convolution in the r-direction and $\overline{\ell}$ is the first moment of $\phi(\ell)$. Equation (19) demonstrates the fact that the two distribution densities $\phi(r)$ and $f(r)$ define $\gamma''(r)$. On the other hand, it is not possible to determine $\phi(r)$ and $f(r)$ from the one and only experimental function $\gamma''(r)$. Additional geometric information is welcome here. Certainly, f can be eliminated from equation (19), if γ'' and ϕ are known. This can be useful in practice if the particle shape is known, see [18]. The $f(m)$-result is a sequence of convolution-terms including δ-functions.

$$f(r) = [(1-p)\overline{\ell}\gamma''(r) + 2\delta(r) - \phi(r)]* \\ [\delta(r) - (1-p)\overline{\ell}\gamma''(r)*\phi(r) + (1-p)\overline{\ell}(\gamma''(r)*\phi(r))^{2*} - ... + ...]. \tag{20}$$

Really, in equation (20) f and ϕ may be exchanged; ϕ corresponds to p and f corresponds to $1-p$.

4.3 Example: A linear system with l_1=l_2=3=const., m_1=2=const.

The interpretation of the behaviour of $\gamma(r)$ and $\gamma''(r)$, defined by equations (19, 20), is demonstrated for a simple surveyable case in Figure 11. Two one-dimensional particles of size 3, separated by a gap of length 2 in a system of length 8 (r-interval $0 \le r \le 8$), are studied. The particle indicator function $\mathbf{i}(r)$ is given by: $\mathbf{i}(r) = 0$, if $3 < r < 5$, else $\mathbf{i}(r) = 1$. The meandensity is 6/8. $\gamma(r)$ is the normalized convolution square of the density fluctuations, see equation (21), Debye and Bueche [33]

$$\gamma(r) = \frac{\int_0^L \eta(x+r)\eta(x)\mathrm{d}x}{\int_0^L \eta^2(x)\mathrm{d}x}\,. \tag{21}$$

4.4 Chord lengths in a Boolean model with spherical primary grains

Another case, in which detailed analytic expressions of equations (19, 20) are known, is a so-called Random Closed Set (RACS), see Serra [2], Hermann [34]. Compact expressions for $\gamma(r)$ exist, see [35]. The mean chord

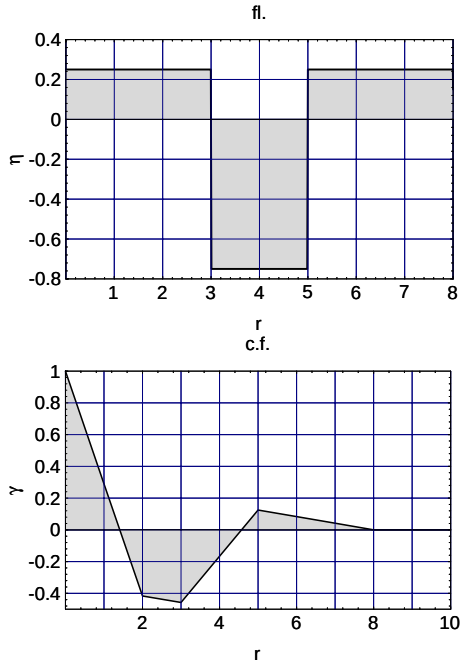

Fig. 11. The (electron) density fluctuation, fl. $\eta(r)$, defines a finite linear two-phase system with the order distance $L = 8$ and volume fraction $p = (\ell_1 + \ell_2)/L = 75\%$. $\gamma''(r)$ consists of five δ-terms: At $r = 0$ and $r = m_1$, $r = \ell_1 = \ell_2$ and $r = \ell_{12} + m_1$ and $r = L$, see equation (19). The function $\gamma''(r)$ of each tightly packed system involves both MCD-terms and OCD-terms. There exists a positive OCD-term at $r = L = 8$, $\gamma''(L) > 0$. The peak at $r = 5 = \ell_1 + m_1 = \ell_2 + m_1$ possesses a "curvature" to the right, $\gamma''(5) < 0$. This reflects a negative OCD-term, see the position $r = \ell_1 + m_1 = 25$ nm in Figures 19, 20.

lengths in both phases are

$$\overline{\ell} = \int_0^L \ell\phi(\ell)\mathrm{d}\ell = -\frac{\exp(N)}{\gamma'(0)}, \\ \overline{m} = \int_0^L mf(m)\mathrm{d}m = -\frac{1}{(1-\exp(-N))\gamma'(0)},\ N = \lambda V_0. \tag{22}$$

In the *Boolean model*, for details see [1,2], $\gamma(r)$ depends on $\gamma_0(r)$, the c.f. of the primary particles (p.pa.) with mean volume V_0. The variable λ is the intensity of the Poisson process (number of primary particles per volume). In the limiting case of an infinitely diluted system $\gamma(r) = \gamma_0(r)$ holds. Then $\lambda \to 0$, $N \to 0$, $p = 1 - \exp(-N) \to 0$. The mean average μ-chord length d of the particle system is

$$d = \frac{\overline{\ell} + \overline{m}}{2}\,. \tag{23}$$

Figure 12 shows a cubic section of such a set, constructed from 20 primary points and the corresponding spherical primary particles, in a test volume of 10^3, with the parameters: $\lambda = 0.02$, $N = 0.223$, $p = 20\%$. The diameters D_i of the p.pa.'s are evenly distributed in the D-interval

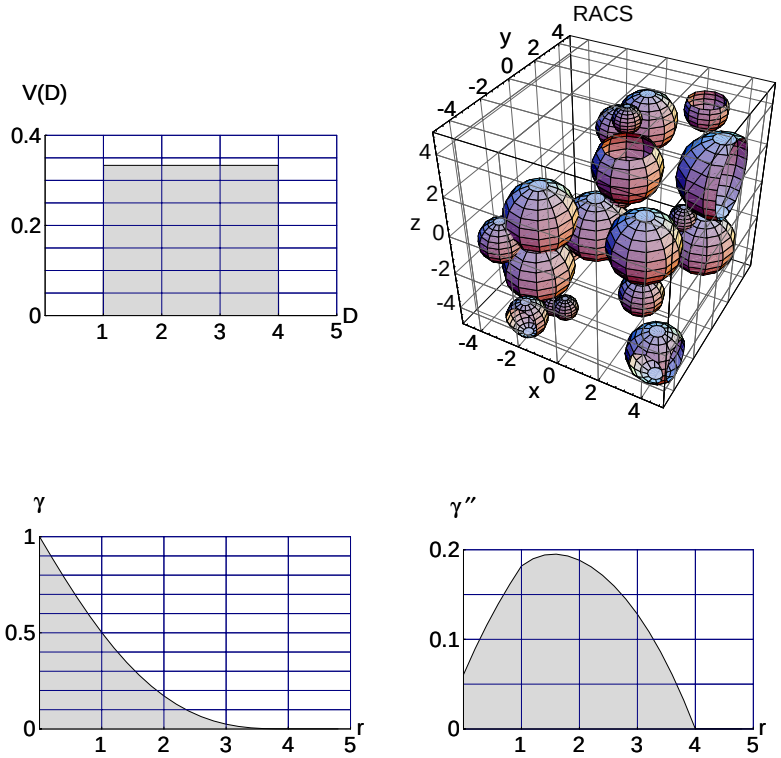

Fig. 12. A geometric simulation of a *Boolean model* with the corresponding structure functions. The functions γ and γ'' are non-negative for such systems. The limiting values $\gamma'(0) = -0.5511$ and $\gamma''(0) = 0.0606$ define p; $p = \gamma''(0)/[\gamma'(0)]^2$ see [35].

$1 < D < 4$, see $V(D)$ in Figure 12. The average volume of the p.pa.'s is about 11. There exists a short-range order L (L is the biggest dimension of the biggest p.pa.). Thus, $V(D)$ produces $L = 4$ in this type of model.

5 The determination of c.l.d.'s from SAS-experiments

All methods of structural interpretation of SAS data mainly deal with a precisely recorded intensity curve (2% noise or less) on high-precision h_k-abscissas. Then, the calculation of γ, γ_1, γ'' from SAS-curves, see for example Feigin and Svergun [10], is no problem for specialists of numerical mathematics today. There exist a lot of methods which are applicable for common laboratory-experiments as well. Modern computational systems, like *Mathematica* [36], are the toolkit used in the laboratories. In the following, three typical examples for the transformation from $I(h)$ to $\gamma''(r)$ are explained. The experimental information is based on the data $I_k(h_k)$ given on discrete points in a limited h-interval, $h_{min} < h < 1.5/\text{nm}$.

One specific test simulation (determination of $A(\ell)$ for a single sphere), a *typical scattering curve from the field of porous substances* (silica aerogel scatterer, tightly-packed two-phase system with $L = 20$ nm), and an *example from polymer physics* (lamellar structure of a low-density-polyethylene Buna-PE 539 sample, $L = 35$ nm). For details about Figure 15, see Schaefer [37].

The resulting functions γ and $\gamma''(r)$, calculated from a simulated $I_k(h_k)$-experiment ($N = 30$ points, $h_{min} = 0.05/\text{nm}$, $h_{max} = 1.5/\text{nm}$, 3% noise of I_k and 2% noise of h_k), are given in Figures 13–14. Instead of an extrapolation of $I(h)$ for $h \to \infty$, "*backward extrapolation*" (see below) was applied. Figure 14 shows beside the numerical result the theoretical one. Experience in this

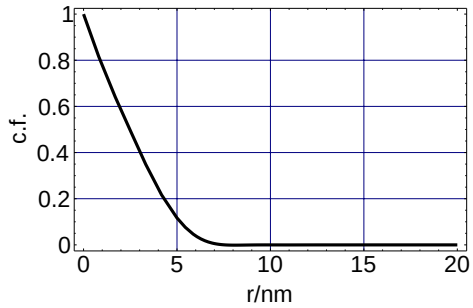

Fig. 13. The c.f. of a $L = 7$ nm-sphere.

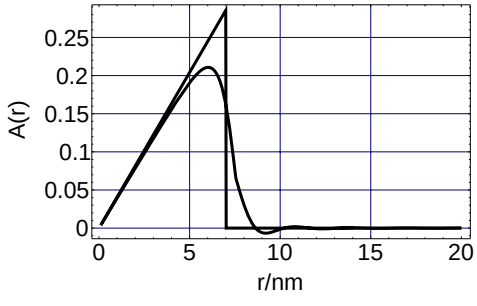

Fig. 14. $A(r)$ calculated from simulated data.

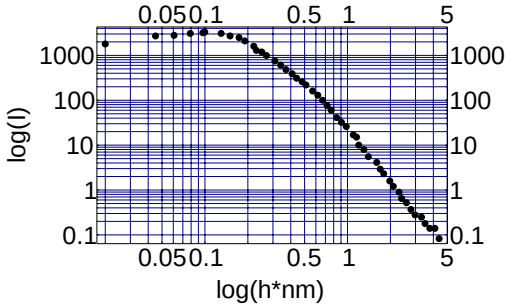

Fig. 15. $I(h)$ from a porous silica aerogel.

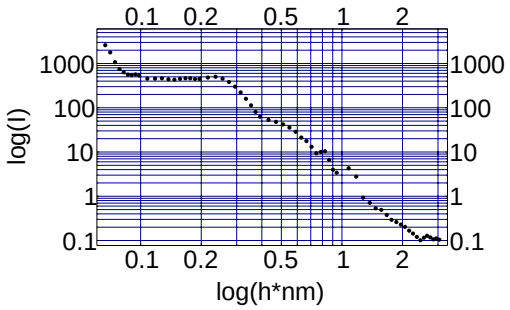

Fig. 16. $I(h)$ of PE 539, author measurement.

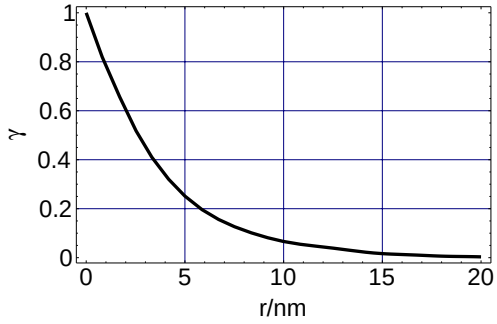

Fig. 17. The c.f., corresponding to Figure 15.

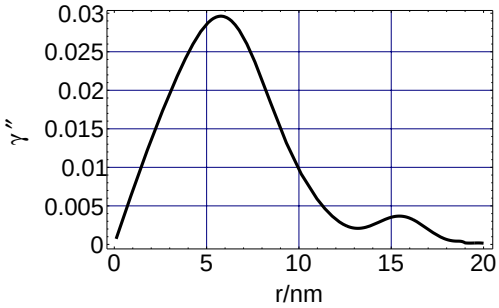

Fig. 18. γ'', calculated from $I(h)$, Figure 15.

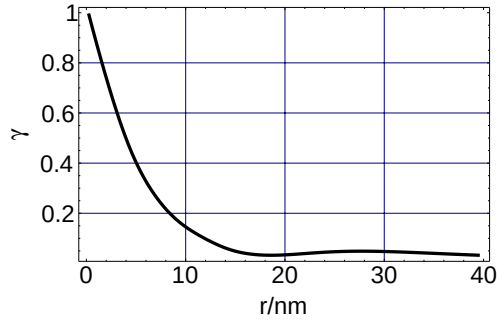

Fig. 19. The c.f. of the PE-sample.

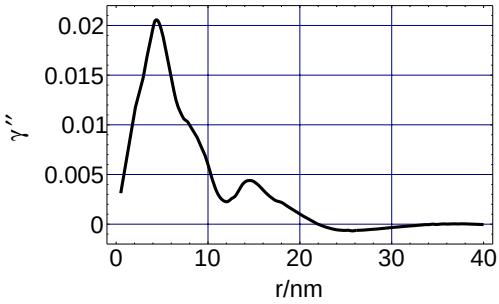

Fig. 20. $\gamma''(\phi(r)$ and $f(r))$ of the PE-sample.

field shows that from an SAS-precision experiment much better results than in Figures 13–14 can be expected (smaller noise and $N > 30$ recorded $I_k(h_k)$-values). The sphere-simulation-test case is by far one of the most fastidious tests. Likewise, γ and γ'', see Figures 17–18, were obtained from the two following experiments Figures 15, 16.

The peaks of γ'' in Figure 18 approximately correspond to the mean chord length in the air-phase and the solid-phase of the sample, $L = 20$ nm. Thus, from the mean chord lengths of the pores, 6 nm, and of the solid phase, 15 nm, follows $c = 6/21$ and $1/\gamma'(0) = -4.3$ nm. The latter can be obtained from the c.f. in Figure 17, too.

The first peak of γ'' in Figure 20 characterizes the c.l.d., $\phi(\ell)$, of crystalline lamellas (the shoulder is connected with a so-called intermediate lamella). The second main peak represents the c.l.d. $f(m)$ of the gaps between the lamellas. The main negative peak, $r = 25$ nm, corresponds to the sums of the segments $\ell_i + m_i$, see Figures 10, 11 and equation (19).

The corresponding interface distribution function $g(r)$, Stribeck and Ruland [38], $g(r) = [3\gamma''(r) + r\gamma'''(r)]/2$ was computed and discussed in [39]. Here, $g(r)$ has a lot in common with $\gamma''(r)$. This is based on the following fact. Considering a straight line (IUR-orientation) in a tightly packed arrangement of lamellas, it can be observed that the heights of the lamellas, and also of the interspaces, are directly proportional to both types of chords ℓ_i and m_i, which result here; see the singularities in curvature of $\gamma(r)$ in Figure 11.

The structure functions in Figures 13–14, 17–18, 19–20 were obtained without application of any "final-γ''-smoothing procedure". A direct procedure of data evaluation, named "*backward extrapolation*", see [18,19], was

used. It is based on the transition function $t(r, h_u)$ of a parametric integral defined by

$$t(r, h_u) = \int_0^{h_u} I(h)K(r, h)\mathrm{d}h, \quad 0 \le h_u \le h_{max}. \quad (24)$$

In the parametric integral, equation (24), the experimental function $I(h)$ occurs together with an oscillating kernel $K(r, h)$, which is known exactly. In typical cases K is given by $K(r, h) = \sin(hr)/(hr)$ or by $K(r, h) = \cos(hr)$ or by the corresponding Bessel functions. Usually $t(r, 0) = 0$ holds. It is obvious that $t(r, h_{max})$ does not lead to the best approximation. K oscillates and gives positive and negative values (in some cases a fixed period $2\pi/r$ occurs). Therefore, also $t(r_0, h_u)$ is oscillating. For each constant r, the integral is approximated considering the most probable value of the function $t(r, h_u)$ for h_u in the interval $0 < h_u < h_{max} = 1.5/\mathrm{nm}$. This can be handled by statistical methods, for example by analysis of the first moment of the distribution density of the t-values (t is then considered to be a random variable).

In cases $r < \pi/h_u$ the "information content" of t in terms of h_u is too small to enable a precise estimation. This is in complete agreement with the sampling theorem of information theory. On the other hand, an atom-complex of about 1 nm diameter or smaller (a sharp size-limit does not exist) is not a smooth particle.

6 The maximum particle diameter L

The largest particle diameter L is the upper integration limit of all integrals in real space in the whole field of SAS. Therefore, L should be estimated by use of all experimental methods evaluable before the first step of each SAS-data evaluation procedure. This holds for direct transformation procedures as well as for indirect ones, Feigin and Svergun [10].

There are cases, in which L of a single isolated particle can be excellently identified, considering the structure functions $\gamma(r)$, $r^2p(r)$ or the c.l.d. of the particle; but this does not work in all cases. Sometimes the L-determination fails, operating with a simple γ-plot, demonstrated in the left-hand part of Figure 21.

6.1 The L-parameter as a special chord length

It is a long-standing problem to analyze the behaviour of the c.l.d. of a single, isolated particle for the so-called "extremal chords" (e.c.'s) of the particle. The e.c.'s are a bit shorter than L, $\ell = L - \varepsilon$. General shape-independent analytical results are based on an approximation of the particle surface in the two extreme points using the principal curvatures, see Gille [40]. The results, see Table 1 in the next section, are highly-symmetrical square root expressions which coincide with the limiting results of an ellipsoid.

Table 1. Representation of $A(L)$ and $A'(L)$ for a single particle in two and three dimensions, see [40].

Surface approximation in with	$A(L)$	$A'(L)$
R^2 2 curvatures	$+\frac{\overline{\ell}}{S_0}\frac{g(D_1,D_2)}{a(D_1,D_2)}$	$-A(L)\left[\frac{2}{D_1+D_2}+\delta(\ell-L)\right]$
R^3 2 curvatures	0	$-\frac{\pi}{2}\frac{\overline{\ell}}{V}\left(\frac{g(D_1,D_2)}{a(D_1,D_2)}\right)^2$
R^3 4 curvatures	0	$-\frac{\pi}{2}\frac{\overline{\ell}}{V}\frac{g(D_{o1},D_{u1})}{a(D_{o1},D_{u1})}\frac{g(D_{o2},D_{u2})}{a(D_{o2},D_{u2})}$

In the case of three-dimensional figures, besides $\gamma(L) = 0$, $\gamma'(L) = 0$ also holds true. Singularities in $A(\ell) \sim \gamma''(\ell)$ only occur in the special case in which all mean curvatures in the two intersection points of the e.c.'s are exactly the same. This is the case with a single sphere. The next section considers a more general case.

6.1.1 A'(L) for two- and three-dimensional figures

The study of the behaviour of $A(\ell)$ for the e.c.'s gives the following results in terms of the curvature of the considered particle near the e.c., having an upper and a lower end. In the most general case of ellipsometry, $A'(L)$ is given in terms of four parameters, two upper $\{D_{u1}, D_{u2}\}$, and two lower $\{D_{o1}, D_{o2}\}$, mean curvature diameters. It holds that, see [19]:

$$A'(L) = -\frac{\pi}{2}\frac{\overline{\ell}}{V}\frac{\sqrt{D_{o1}D_{u1}}\sqrt{D_{o2}D_{u2}}}{L}\frac{1}{\sqrt{L-\frac{1}{2}(D_{o1}+D_{u1})}} \times \frac{1}{\sqrt{L-\frac{1}{2}(D_{o2}+D_{u2})}}. \quad (25)$$

In equation (25), L extends from the lower particle end (index $o_{1,2}$) to the upper one (index $u_{1,2}$). $A'(L)$ is fixed in terms of the curvatures at the particle ends. Moreover, Table 1 shows the connections in six cases in a more compact form.

The abbreviations in Table 1 are the functions g and a, defined by the mean values:

$$g(x, y) = \sqrt{\frac{xy}{L}}, \quad a(x, y) = \sqrt{L - \frac{x+y}{2}}.$$

All relations are symmetrical with respect to the geometric and arithmetical means $g(x, y)$ and $a(x, y)$. The $A(\ell)$ functions considered in the Figures 2–5 and 7, 9 possess the properties given in Table 1.

In addition, a far-reaching analogy between the results in the plane and those in space is notable in Table 1. In the transition from plane to space, each new curvature possible is represented by one new square root term. Further, for each of the curvature parameters D_c in Table 1, $0 \le D_1, D_2, D_{o1}, D_{o2}, D_{o2}, D_{u1}, D_{u2} < \infty$ holds.

Considering any limiting case $D_c \to 0$, the considered terms $A(L)$ and $A'(L)$ disappear. Then, it is no use trying to determine L by differentiating the c.f. In order to determine L in such a case, other methods must be used, see Müller *et al.* [41] or the transformation explained in Section 6.2.

Such an exceptional geometric figure, in which L cannot be detected by equation (25) or by Table 1, is the cuboid.

6.1.2 A'''(L) for the cuboid

The c.l.d. of a cuboid (edges a, b, c, $0 < a < b < c < \infty$) was considered, see [27]. The corners at the end of the space-diagonal of length $L = \sqrt{(a^2+b^2+c^2)}$ correspond to $D_o = D_u = 0$. Consequently, in agreement with equations (25, 26) and Table 1, $A(L) = 0$ and $A'(L) = 0$ results. Further, from equation (26), which represents $A(r, a, b, c)$, anew follows $A''(L) = 0$.

$$
\begin{aligned}
&A(r,a,b,c) = \\
&\frac{8}{\pi S}\left\{-\frac{3}{4}r + \frac{1}{r^3}\left[\frac{a^4+b^4+c^4}{12} - \frac{a^2b^2+a^2c^2+b^2c^2}{2}\right.\right. \\
&\left. + \; aF(s_a) + bF(s_b) + cF(s_c)\right] \\
&+\frac{abc}{r^3}\left[+a\left(\arctan\left(\frac{c}{\sqrt{r^2-s_b^2}}\right) - \arctan\left(\frac{\sqrt{r^2-s_c^2}}{b}\right)\right)\right. \\
&+ b\left(\arctan\left(\frac{c}{\sqrt{r^2-s_a^2}}\right) - \arctan\left(\frac{\sqrt{r^2-s_c^2}}{a}\right)\right) \\
&\left.\left.+c\left(\arctan\left(\frac{a}{\sqrt{r^2-s_b^2}}\right) - \arctan\left(\frac{\sqrt{r^2-s_a^2}}{b}\right)\right)\right]\right\}.
\end{aligned}
\tag{26}
$$

Abbreviations: $s_c = \sqrt{a^2+b^2}$, $s_a = \sqrt{b^2+c^2}$, $s_b = \sqrt{a^2+c^2}$, $F(x) = \sqrt{r^2-x^2}\left(\frac{x^2}{3} + \frac{2}{3}r^2\right)$, $S = 2(ab + ac + bc)$.

Furthermore, the detailed treatment of the differentiation-project then finally yields a limit $A'''(L) < 0$ for the c.l.d., connected with the two convex corners at the end of the space diagonal. This specific limit is given by equation (27),

$$
A'''(L) = -\frac{4}{\pi}\frac{(a^2+b^2+c^2)^2}{a^2b^2c^2(ab+ac+bc)} = -\frac{8}{\pi}\frac{(a^2+b^2+c^2)^2}{V^2 S}. \tag{27}
$$

This manner of presentation, an extension of Table 1, means that the L-determination by differentiation would require a 5th derivative of $\gamma(r)$ for this geometric figure. Consequently, another strategy must be pursued to determine the largest particle dimension L, see next section. The case of a steep cone is similar, see [30].

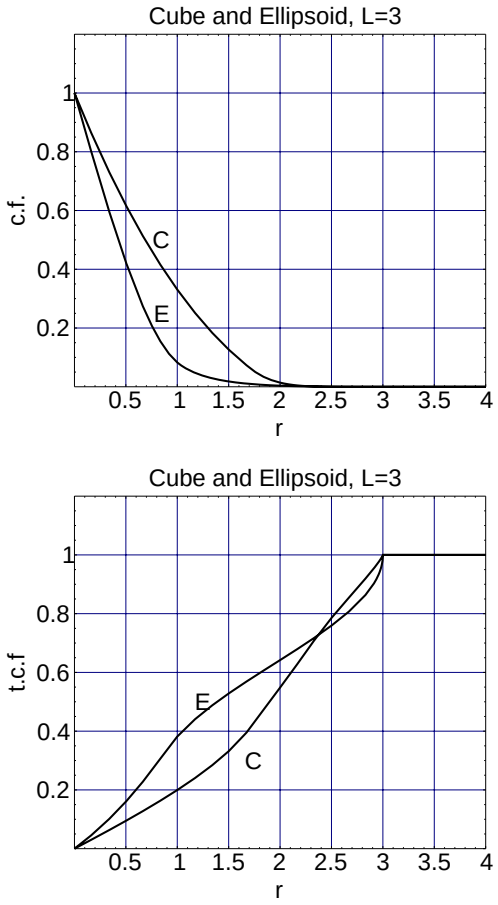

Fig. 21. c.f. and t.c.f. for a cube (curve C) with edge length $\sqrt{3}$ and an ellipsoid (curve E) with semi-axes $\{a = 1, b = 1, c = 1.5\}$. The longest chord is $L = 3$ in both cases. This value follows from the t.c.f., but cannot be detected directly from the c.f.

6.2 Determination of the largest particle diameter L via $\gamma_T(r)$

The last section demonstrates that even in a diluted particle system the determination of L is often complicated. A method, explained and tested with simulated and experimental scattering curves in [41] uses a new integral transform of SAS-data. This method requires a Struve-transform of the scattering data. It is tailormade for the more general case of smeared scattering curves.

Another practicable method to estimate L is the method of the transformed correlation function, t.c.f., $\gamma_T(r)$. This function is normalized similarly to $\gamma(r)$ and defined by:

$$
\gamma_T(r) = \frac{2}{\pi}\arcsin\left(1 - [\gamma(r)]^{\frac{1}{3}}\right), \; 0 < \gamma(r) < 1. \tag{28}
$$

A particular application of equation (28), see also Gille [42], is demonstrated in Figure 21.

In the case of the cube the differentiation of $\gamma(r)$, in order to determine L, does not make sense, see Table 1

and equations (25–27). Nevertheless, the t.c.f. clearly indicates the length of the space diagonal $L = 3$ in the form $\gamma_T(3) = 1$. The comparison of cube and ellipsoid in Figure 21 demonstrates that the c.f. of the cube extremely closely "snuggles" to the axis of abscissas near $r = L - \varepsilon$, much more closely than the c.f. of the ellipsoid, see Table 1 and equations (25–27).

7 Summary

The c.l.d.-concept is by far more than only the discussion of a second derivative of a certain function $f(x) = \gamma(x)$ in the style of a formal curve-discussion. The set of c.l.d.'s, $\gamma''(r)$, contains the peculiarities of all particle borders in a compact form, without being at all influenced by the "inner life" of particles and of particle to particle gaps.

Physical structure functions, which are closely connected with the geometric covariance, can be calculated numerically from SAS-experiments. This includes the determination of an approximation of the c.l.d. of the typical microparticles of interest. The characterization of practically all particle shapes can be completed by comparing the experimentally obtained c.l.d.'s with theoretical ones. The latter requires a large spectrum of c.l.d.'s in an analytic form. It further requires a theory which includes particles with hollow regions (MCD-case and OCD-case) and tightly packed particle arrangements (simultaneous consideration of the basic dependencies between the three structure functions $\phi(\ell)$, $f(m)$, $\gamma''(\ell)$). The MCD-case is the classic situation of geometric models in SAS. But, for tightly packed systems $\gamma''(\ell)$ reflects OCD-distances as well. MCD-distances produce always positive peaks. Otherwise, OCD-distances produce negative terms of γ'', if the number of chord segments in the sum $(\ell_1 + m_1) + (\ell_2 + m_2) + ...$ is even. OCD-distances produce positive terms of γ'', if the number of chord segments in the sum $\ell_1 + m_1 + \ell_2 + ...$ is unpaired.

The step from the experiment to the c.l.d. requires concentration upon a limited h-interval, $h < \pi/(1.5\ \text{nm})$, in all steps of experiment and data evaluation. The question, how exactly must an experiment be performed in order to calculate γ'', can be answered, independent of the used function-system in the numerical data evaluation, in a simple way: $I(h)$ must be measured accurately enough so that $I''(h)$ can be calculated from these data. Then, the c.l.d. can be determined, *e.g.* by use of equation (3) by way of a smoothing h-integration. But, equation (3) combined with the "backward extrapolation" is *by far not* the only possible way for reducing the truncation errors. Worldwide, there are a lot of excellent numerical packages for data treatment and data evaluation in this field, see also the special packages of the *Mathematica* program [36], Signals and Systems.

The determination of the largest particle diameter L by differentiating $\gamma(r)$ for a single particle works in cases where there are finite principal curvatures in the particle points farthest apart. The consideration of the sequence $\{\gamma(L),\ \gamma'(L),\ A(L),\ A'(L), ...\}$ does not allow the estimation of L if infinite curvatures in the most distant particle points exist. Here, the t.c.f.- method can be applied to determine an approximation of one or (in exceptional cases) more range-orders L_i.

If the principal curvatures in each endpoint of L have finite values, a large spectrum of $A(L)$-cases and $A'(L)$-cases of geometric figures can be evaluated, as outlined in Table 1. Moreover, Table 1 indicates possibilities for the characterization of the principal curvatures of microparticles of disperse materials from scattering experiments.

References

1. D. Stoyan, W.S. Kendall, J. Mecke, *Stochastic Geometry and Its Applications* (Akademie Verlag, Berlin, 1987).
2. J. Serra, *Image Analysis and Mathematical Morphology* (Academic Press, London, 1982).
3. U. Mäder, Radiat. Res. **82**, 454 (1980).
4. E.R. Weibel, *Stereological Methods*, Vol. 2 (Academic Press, London, 1980).
5. R. Hilfer, Adv. Chem. Phys. **XCII**, 299 (1996).
6. R. Hilfer, Phys. Rev. B **44**, 60 (1991).
7. A.J. Cabo, A.J. Baddeley, Adv. Appl. Prob. (SFSA) **27**, 585 (1995).
8. D. Stoyan, H. Stoyan, *Fraktale Formen Punktefelder* (Akademie Verlag, Berlin,1992) p. 135.
9. A. Guinier, G. Fournet, *Small-Angle Scattering of X-Rays* (John Wiley & Sons,New York, 1955).
10. L.A. Feigin, D.I. Svergun, *Structure Analysis by Small-Angle X-Ray and Neutron Scattering* (Plenum Press, New York, 1987).
11. D. Tchoubar, *Diffusion centrale des Rayons X par les Systmes Poreux*, thesis, Paris 1967.
12. W. Gille, J. Phys. IV Colloq. France **4**, C8-503 (1994).
13. R. Sobry, J. Ledent, F. Fontaine, J. Appl. Cryst. **24**, 516 (1991).
14. R. Sobry, *Details of the asymptotic expansion of $I(h)$* (private communication, 1998).
15. S. Ciccariello, J. Math. Phys. **36**, 219 (1995).
16. G. Damaschun, H.-V. Pürschel, Monatshefte Chemie **100**, 247 (1969).
17. B. Lu, S. Torquato, J. Chem. Phys. **98**, 6472 (1993).
18. W. Gille, *Stereologische Charakterisierung von Mikroteilchensystemen mit der Kleinwinkelstreuung*, thesis, Halle 1983.
19. W. Gille, *Das Konzept der Sehnenverteilung zum Informationsgewinn aus einer Kleinwinkelstreukurve und seine Grenzen*, Habilitationsarbeit, Halle 1995.
20. A. Rosiwal, Verh. K.K., Geol. Reichsanst. **5/6**, 143 (1898).
21. E. Enns, P. Ehlers, JAP **15**, 144 (1978).
22. M. Teichgräber, thesis, Technical University Leuna-Merseburg, 1971.
23. D. Fanter, thesis, Institute of Polymer Chemistry, Teltow-Seehof, 1977.
24. A.M. Kellerer, Radiat. Res. **47**, 359 (1971).
25. T.B. Borak, Radiat. Res. **137**, 346 (1994).
26. W. Gille, Exp. Tech. Phys. **35**, 93 (1987).
27. W. Gille, Exp. Techn. Phys. **36**, 197 (1988).

28. W. Gille, H. Handschug, *The chord length distribution of a hemisphere*, internal report, Martin-Luther University, 102 p., Halle 1993.
29. W. Gille, Comp. Mater. Sci. **15**, 449 (1999).
30. W. Gille, H. Handschug, Math. Comp. Modelling **30**, 107 (1999).
31. W. Gille, J. Appl. Cryst. **32**, 1100 (1999).
32. G. Porod, *Kolloid Zeitschrift* **124**, 83 (1951); **125**, 51 (1952).
33. P. Debye, A.M. Bueche, J. Appl. Phys. **20**, 518 (1949).
34. H. Hermann, *Stochastic Models of Heterogeneous Materials* (Trans. Tech. Publications, Zürich 1991).
35. W. Gille, Part. Part. Syst. Charact. **12**, 123 (1995).
36. Wolfram Research, Inc., *Mathematica*, versions 3 and 4, Champaign, Illinois 1996/98.
37. D.W. Schaefer, *X-ray scattering curve of a porous silica aerogel of density 0.36 g/cm^3,* (Sandia Nat. Laboratories, 1993). These data were presented at the NATO Advanced Study Institute on Modern Aspects of SAS. Como/Italy May 12-22.
38. N. Stribeck, W. Ruland, J. Appl. Cryst. **11**, 535 (1978).
39. W. Gille, Direct calculation of the interface distribution function and other structure functions from SAS-curves, Halle, 1998.
40. W. Gille, Comp. Mater. Sci. **15**, 50 (1999).
41. J. Müller, W. Gille, G. Damaschun, *Direct determination of the largest diameter of a particle by a new transformation of X-ray scattering data,* unpublished report, 22 p., Berlin and Halle 1993.
42. W. Gille, Comp. Mater. Sci. **18**, 65 (2000).